Nanoscale

PAPER

View Article Online
View Journal | View Issue

Cite this: *Nanoscale*, 2020, **12**, 7914

In situ formation of H-bonding imidazole chains in break-junction experiments†‡

Chuanli Wu,§[a,b] Aminah Alqahtani,§[c] Sara Sangtarash, *[c,d] Andrea Vezzoli, *[a,e] Hatef Sadeghi, [d] Craig M. Robertson,[a] Chenxin Cai,[b] Colin J. Lambert, *[c] Simon J. Higgins [a] and Richard J. Nichols *[a]

Received 22nd January 2020,
Accepted 18th February 2020

DOI: 10.1039/d0nr00630k

rsc.li/nanoscale

As a small molecule possessing both strong H-bond donor and acceptor functions, 1*H*-imidazole can participate in extensive homo- or heteromolecular H-bonding networks. These properties are important in Nature, as imidazole moieties are incorporated in many biologically-relevant compounds. Imidazole also finds applications ranging from corrosion inhibition to fire retardants and photography. We have found a peculiar behaviour of imidazole during scanning tunnelling microscopy-break junction (STM-BJ) experiments, in which oligomeric chains connect the two electrodes and allow efficient charge transport. We attributed this behaviour to the formation of hydrogen-bonding networks, as no evidence of such behaviour was found in 1-methylimidazole (incapable of participating in intramolecular hydrogen bonding). The results are supported by DFT calculations, which confirmed our hypothesis. These findings pave the road to the use of hydrogen-bonding networks for the fabrication of dynamic junctions based on supramolecular interactions.

1. Introduction

Single-entity experiments[1] and the advancement of computational methods[2] have increased our understanding of the behaviour of matter at the molecular level. A novel approach to the characterisation of individual molecules has been the fabrication of molecular junctions,[3,4] where a single entity is sandwiched between two biased metallic electrodes, and the current flowing through the nanoscale device is used as a characterisation signal. The conductance of a junction is exquisitely correlated with the chemical nature of the molecular wire, and with the support of computational methods, can be used to extract structural, electronic and conformational information. As methods for single molecule electrical characterisation have advanced so have the complexity of molecular systems which can be studied. In recent years this has included the study of molecular assemblies, which has included dimeric molecular pairs and supramolecular assemblies. An example here is the study of pairs of fullerenes in an STM junctions sandwiched between gold electrical contacts, with one fullerene attached to the surface and the other directly on-top and attached to the STM tip.[5] Fullerene functionalised STM tips have also been used to form single porphyrin–fullerene dyads through non-covalent interactions,[6] and π-stacking has also been exploited to assemble molecular pairs in STM break junctions.[7,8] On the other hand, hydrogen bonding is widely exploited in both chemical and biochemical systems for the exquisite assembly of often complex supramolecular structures, but it has only been used in a relatively few single molecule junction studies. Nishino have assembled pairs of ω-carboxyl alkanethiols monolayers onto a gold STM tip and substrate.[9] The carboxylic acid groups of these adsorbates were bound through hydrogen bonding across the junction in an STM electrical junction. Hydrogen bonding across molecular junctions has also been achieved with DNA base pairs and has been used to study hydrogen-bonding dynamics.[10,11] In this contribution we explore new possibilities to exploit hydrogen bonding in nanoscale electrical junctions and show that hydrogen bonding can also be used to form extended chains of molecules spanning the nanogap. We deployed 1*H*-imidazole (1,3-diazole, Fig. 1a) as the molecular

---

[a] *Department of Chemistry, University of Liverpool, Crown Street, Liverpool L69 7ZD, UK. E-mail: andrea.vezzoli@liverpool.ac.uk, nichols@liverpool.ac.uk*
[b] *School of Chemistry and Materials Science, Nanjing Normal University, Nanjing 210023, People's Republic of China*
[c] *Quantum Technology Centre, Physics Department, Lancaster University, Lancaster LA1 4YB, UK. E-mail: s.sangtarash@lancaster.ac.uk, c.lambert@lancaster.ac.uk*
[d] *School of Engineering, University of Warwick, Coventry CV4 7AL, UK*
[e] *Stephenson Institute for Renewable Energy, University of Liverpool, Peach Street, Liverpool L69 7ZF, UK*

† Data collected using EPSRC funding at Liverpool are archived at DOI: 10.17638/datacat.liverpool.ac.uk/968

‡ Electronic supplementary information (ESI) available: Additional STM-BJ experiments on benzimidazole and in heavy water, additional DFT and transport calculations. See DOI: 10.1039/d0nr00630k

§ These authors contributed equally to this work.

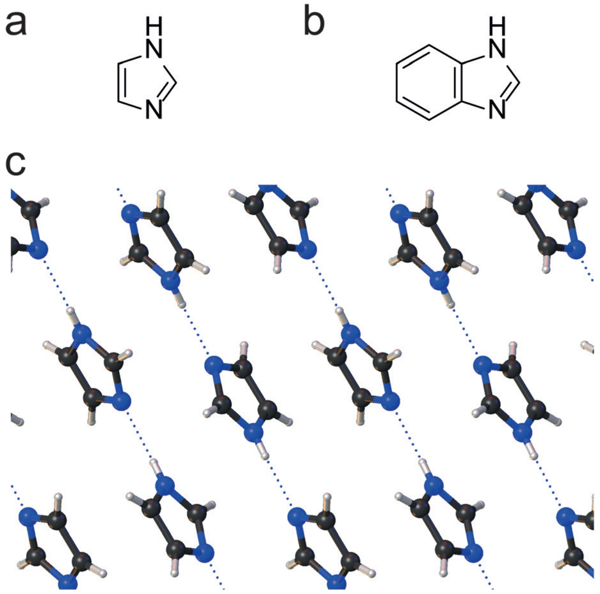

Fig. 1 (a) Structure of 1*H*-imidazole and (b) benzimidazole. (c) Crystal structure of 1*H*-imidazole along the (010) crystallographic plane, showing the NH⋯N hydrogen bonding motif. Structure retrieved from the Cambridge Crystallographic Data Centre, entry IMAZOL03, deposition #136337.

target and exploited the versatility of STM single-molecule electrical characterisation to study its behaviour of at noble metal interface.

1*H*-Imidazole is a simple 5-membered heterocyclic aromatic compound with amphoteric properties, and a structure of both biological (*e.g.* histidine, miconazole, purine) and technological (*e.g.* transition metal corrosion inhibitor, ionic liquids, fire retardants) importance. Many of its relevant properties arise from its high electric dipole moment (3.67 D) and its ability to form strong H-bonding networks both in the solid state[12] and in solution.[13] This results, for instance, in 1*H*-imidazole itself being a crystalline solid at standard temperature and pressure, with a relatively high melting point of 89–91 °C despite its low molecular weight. In the solid state, 1*H*-imidazole forms one-dimensional molecular networks, linked by NH⋯N intermolecular hydrogen bonds[14,15] which are in essence very long coordination polymers (Fig. 1c) with a persistent tape motif.[16]

Through the H-bonding axis (*c* crystallographic plane), charge transport of solid state 1*H*-imidazole crystals is $>10^3$ times more efficient than along the other two axes.[17] This strong electrical anisotropy is mirrored in the shape of the crystal themselves, which are long and fragile fibrous needles. Imidazolic compounds also form a range of complexes with alkali and transition metal cations, *via* interactions of the lone pair electrons on the imine nitrogen. H-Bonded coordination networks are formed in the complexes, either between the imidazolic nitrogens[18] or through interactions with water[19] or carboxylic acid functionalities,[20] highlighting the particular strength and resilience of such networks. The complexing properties of imidazolic compounds are further evidenced by their ability to adsorb at transition metal surfaces and passivate them. This phenomenon is exploited in their wide use as corrosion inhibitors. The structure of imidazolic films at metal surfaces is complex, with the passivating film thickness and arrangement depending on the deposition conditions and *N*-substituents. As an illustrative example for its behaviour with coinage metals, 1*H*-imidazole etches the surface of copper to give coordinating species. Tri- and tetrameric fragments are formed, which are bound together with the substrate.[21] Raman spectroscopy suggests the adsorption proceeds mainly through interactions of the sp^2 N atom with the metal surface, coordinated through its lone electron pair, with the ring perpendicular (or at a small tilt angle) to the surface.[22] However, a parallel deprotonation mechanism, with formation of imidazolate–metal bonds, is evident in *in situ* infrared spectroscopy.[23] Recently, it has also been successfully used as a molecular contact in scanning tunnelling microscopy break junction (STM-BJ) studies, as an aurophilic terminus.[24]

We came across an anomalous behaviour of imidazolic compounds during our single-molecule conductance studies. In its protonated form, we would not expect junctions to form since the pair of electrons on the pyrrolic nitrogen are part of the aromatic sextet and thus not obviously available for bonding to a metal contact. The pair of electrons on the iminic (pyridine-like) nitrogen is not part of the aromatic sextet and thus "available", but this gives only one anchoring group, not the usual two needed for the formation of robust metal–molecule–metal junctions. On the other hand, a deprotonation of the pyrrolic nitrogen with formation of imidazolate–metal bonds as mentioned above opens the possibility to form bridging junctions across metallic nanogaps. These then might be expected to give a well-defined high conductance value for the imidazolate, similar to what has been observed for pyrazine[25,26] (1,4-diazabenzene), with clear signatures of charge transport through the molecule anchored between the two electrodes by the N atoms in the 1,3-positions, spaced 2.2 Å apart. In what follows, we will show that 1*H*-imidazole and benzimidazole (bicyclic fused benzene and imidazole, Fig. 1b) are indeed capable of forming single-molecule junctions, but as the junctions are pulled apart, conductive H-bonding chains of length greatly surpassing the single-molecule N⋯N distance assemble between the two electrodes, and the structure and charge transport characteristics of these is dependent on the experimental medium.

2. Results and discussion

2.1. Scanning tunnelling microscopy break junction measurements

We fabricated molecular junctions and characterised their behaviour with the *in situ* STM-BJ technique.[3] In this method, a Au tip, in a solution of the target molecule, is driven towards a Au substrate under constant bias until it crashes and forms a metallic contact, with a conductance of several quantum units

($G_0 \cong 77.48$ μS). The tip is then withdrawn at constant speed, until the nanocontact is broken into two sharp nanoelectrodes. Molecules can then self-assembled in the freshly formed nanogap (estimated as approximately ~6.5 Å (±2.5 Å) at room temperature due to snapback[27,28] effects), and the conductance ($G = I/V_{BIAS}$) is recorded as the tip is further retracted, thereby giving a current *vs.* distance (I_z) trace. In a typical trace, several plateaux at conductance values $\geq G_0$ are usually observed, which is a characteristic of charge transport through integer numbers of Au atoms. On the other hand, plateaux appearing at conductance $\ll G_0$ arise from charge transport across the molecular bridge. The process is repeated thousands of times and all the I_z traces obtained are compiled in one-dimensional histograms and two-dimensional conductance maps (no data selection). Plateaux in the I_z traces result in peaks in the histogram, which are then fitted to a Gaussian distribution to quantify the most probable conductance value. High-counts areas in the two-dimensional maps are used to correlate conductance and junction length, thereby giving information about junction evolution processes as the electrodes are pulled apart.

We initially found an anomalous behaviour of 1*H*-imidazole when we measured its conductance in a dry liquid medium (1 mM in degassed, anhydrous mesitylene : tetrahydrofuran 8 : 2 v : v mixture). The conductance histograms (Fig. 2a) shows multiple conductance contributions, spaced by approximately 2 Å as can be observed in the conductance *vs.* distance map in Fig. 2c. These features, after adding the electrode snapback,[28] extend beyond the theoretical size of a single-imidazole junction (approximately 5 Å), thus suggesting the formation of supramolecular entities as the single-entity junction is stretched further. This formation of conductive junctions that extend beyond the length of a single 1*H*-imidazole molecule in anhydrous environment can be rationalised by the formation of oligomeric chains, with junctions incorporating up to three molecules (Fig. 2e), held together by strong hydrogen bonds. At this stage we tentatively assign these three peaks under anhydrous conditions to monomer (labelled M), dimer (D) and trimer (T) 1*H*-imidazole species; this assignment is supported by theoretical modelling presented in the next section (see Fig. 4 for these proposed structures). Each of these structures features deprotonation of the pyrrolic nitrogen with formation of imidazolate–gold bonds. The following computational section shows that deprotonation of the surface-contacting pyrrolic nitrogen gives much more favourable contact binding energies over structures that retain these hydrogens.

Repeating the measurement in Milli-Q water (Merck Millipore ultrapure ISO3696 Type 1) gave a completely different conductance profile (Fig. 2b), again with multiple contributions and junctions which extend even further beyond the molecular length of 1*H*-imidazole (Fig. 2d). In water, a similar H-bonding mechanism could lead to the formation of chains of alternating imidazole and water molecules (Fig. 2f). We have labelled the peaks in the histogram in Fig. 2b as M_{H_2O}, M'_{H_2O}, D_{H_2O} and D'_{H_2O}, which represent the monomer, and dimer peaks, respectively, with the H_2O superscript highlighting that these peaks occur for the measurements in water. Note that the 1D and 2D histograms in Fig. 2 are significantly different in the absence and presence of water, respectively. For the experiments performed in water no peaks in the histogram (Fig. 2b) are attributed to water-containing trimeric oligomers, since as will be shown in the next section, these are predicted to have conductance values several orders of magnitude below the noise floor.

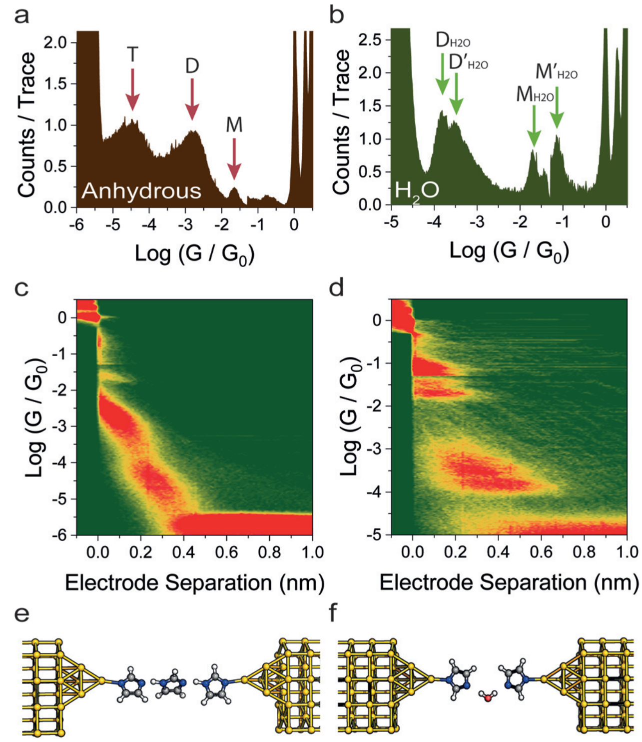

Fig. 2 Summary of experimental results. Conductance histogram of 1*H*-imidazole in an anhydrous environment (a) and in Milli-Q water (b). Two-dimensional conductance *vs.* electrode separation maps for 1*H*-imidazole in anhydrous environment (c) and Milli-Q water (d). Schematic depiction of the H-bonding networks formed by 1*H*-imidazole in an anhydrous environment (e) and Milli-Q water (f). All experiments performed at 200 mV bias. Histogram compiled with 100 bins per decade. Two-dimensional maps compiled with 100 bins per conductance decade and 100 bins per nm. Junction structures in (e) and (f) optimised by DFT energy minimisation (see methods for more details).

As a control experiment, we have performed measurements in deuterated water, which resulted in a broadly similar pattern of multiple peaks. Although the peaks appear at slightly different values of conductance, the differences are smaller than the experimental uncertainty. Within a phase coherent tunnelling model we would not expect an isotope effect and indeed within the error limits and broadness of the conductance peaks none is attributable. Further measurements were then performed with benzimidazole and a similar behaviour was found (more details in the ESI‡). As a further control experiment, we also performed measurements on 1-methylimidazole in anhydrous mesitylene : tetrahydrofuran (8 : 2, v : v), in which intermolecular hydrogen bonds cannot

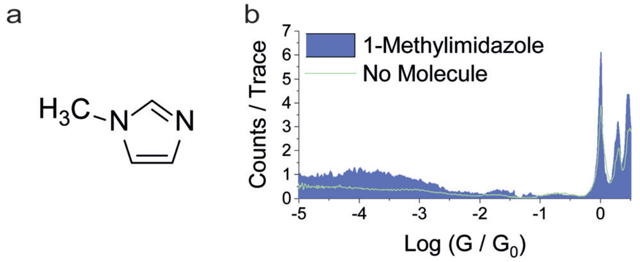

Fig. 3 (a) Structure of 1-methylimidazole. (b) Conductance histogram for 1-methylimidazole recorded under anhydrous conditions (mesitylene : THF, 8 : 2, v : v).

form owing to the lack of a suitable H-bond donor.[29] STM-BJ experiments resulted in no discernible conductance peak (Fig. 3), but only a broad, raised noise level at low conductance values. 1-Methylimidazole readily adsorbs on noble metal surfaces[30,31] through interactions with the lone pair on the sp^2 nitrogen, which would account for the increased tunnelling noise signal, but does not form well-defined junctions between two Au electrodes as the molecule lacks a second contact group (more details in the ESI‡). Evidence of 1-methylimidazole adsorption on the metallic electrode is further provided by the increased G_0 signal, as adsorbates are known to stabilise point contacts.[32] We found no evidence of formation of π-stacked junctions as previously described in the literature,[24] and we ascribe this phenomenon to the different environment used in our study, where tetrahydrofuran can form a solvation shell around the imidazole and prevent the formation of π-stacked supramolecular structures.

2.2. Theoretical modelling

To provide a framework for the interpretation of the data obtained from STM-BJ experiments, we performed density functional theory (DFT) and transport calculations (more details in the Methods section). We started by obtaining the relaxed geometries for 1*H*-imidazole oligomers, in the gas phase and in a nanoelectrode junction. The predicted hydrogen bond length in the gas phase (1.76 Å) is in good agreement with the value found in the solid state (2.04 Å) and the literature.[33] When imidazolic chains are confined within two nanoelectrodes, our calculations predict deprotonation of the imidazole, with formation of a strong Au–N coordination bond, that grants a high electronic coupling. We then calculated the $T(E)$ curves (transmission coefficient as a function of energy, Fig. 4c) for the supramolecular junctions. The conductance of a molecular wire can be directly calculated from these curves *via* the Landauer formula[34] which at a low enough temperature reduces to $G = G_0T(E_F)$, where E_F is the Fermi level of the electrodes representing the energy of the charge carriers tunnelling through the junction from one electrode to the other. Due to known limitations of DFT and the fact that in a STM-BJ experiment a wide range of nanoelectrodes shapes and molecule-electrode geometries are sampled, the most probable value of E_F (relative to the energies of the frontier orbitals) is difficult to estimate. Therefore, it is more accurate to estimate the junction conductance by evaluating the behaviour of $T(E)$ over a range of energies within the molecular HOMO–LUMO gap. Fig. 4 shows the structural models considered in the absence (Fig. 4a) and presence (Fig. 4b) of water and the corresponding computed transmission curves (Fig. 4c and d). The same labelling scheme of monomer (M), dimer (D) and trimer (T) is used for the anhydrous structures and for the water-containing structures, M_{H_2O}, D_{H_2O} and T_{H_2O}. In all cases in Fig. 4 these structures features deprotonation of the pyrrolic nitrogen with formation of imidazolate–gold bonds since this gives much higher contact binding energies than retention of the imidazole hydrogen (*vide infra*). Increasing the number of 1*H*-imidazole units tethered between the two electrodes results

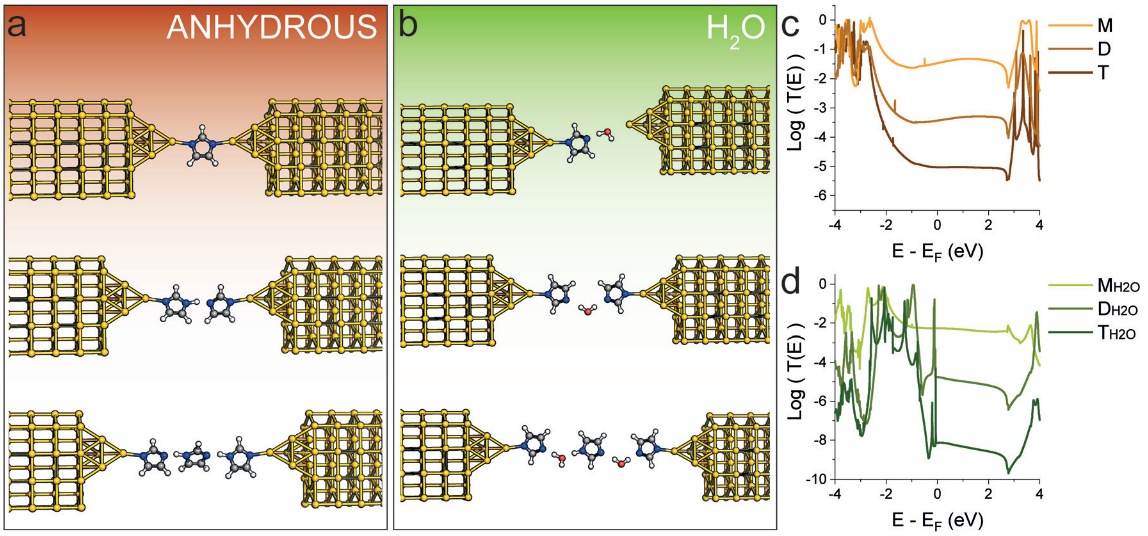

Fig. 4 DFT-optimised junctions of 1*H*-imidazole in (a) anhydrous conditions, with respective transmission curves in (c). (b) Structure of three different 1*H*-imidazole–H_2O supramolecular structures in the junctions, with respective transmission curves in (d).

in a decay of the transmission coefficient (Fig. 4c) which closely matches the experimental values found in the STM-BJ experiments. The calculated conductance values of both the conductance and junction length for monomer (M), dimer (D) and trimer (T) under anhydrous conditions fit very well to the experimental determination.

For the sake of completeness, we also computed $T(E)$ curves when imidazolic N is forced to stay protonated during the junction formation process, and found the same trend (see ESI‡). However, the binding energy of protonated 1*H*-imidazole to Au is quite low, and it is unlikely that junctions could be formed this way. On the other hand, the presence of high-energy, undercoordinated Au atoms on the two nanoelectrodes formed during the break junction process could be the major driving force for N–H dissociation. In contrast, when we tried to model 1-methylimidazole, we found that while it could be a rather inefficient conductor, its binding energy to Au of 50 meV is comparable with the room-temperature value of k_BT, and therefore any junction would be disrupted by thermal fluctuations.

Repeating the calculations in the presence of H_2O molecules yielded different results. Water molecules are efficiently incorporated in the H-bonding chains connecting the two electrodes and increasing the junction length results in a rapid conductance decay (Fig. 4d). An interesting outcome of our calculations is that, to correctly account for the observed break-off distance of the highest conductance peak obtained in water (Fig. 2d), the shortest junction needs to incorporate a single water molecule, adsorbed at the Au electrode and interacting by H-bonding with 1*H*-imidazole adsorbed on the other electrode. Note that the experimental conductance values for the water-containing oligomers are slightly higher than the computed values. Although the computations include water in the molecular bridges, they do not include further hydrations shells surrounding these structures. Therefore, the slightly higher experimental conductance in water solutions could be attributed to an environmental effect. Fatemi *et al.*[35] and Milan *et al.*[36] have previously demonstrated that single molecule measurements performed in different solvents can significantly alter the conductance value. This was explained as a solvent-induced shift of the Fermi level (work function) value, along with an induced dipole upon adsorption of the molecular wire. Hydration shells or solvent-induced shifts of the work function value may also account for the highest experimental conductance peak in water (Fig. 2b) being higher than that under anhydrous conditions (Fig. 2a).

Theory also predicts that, with the sensitivity of our preamplifier (noise level at $\sim 10^{-6} G_0$), we can only measure the monomer and the dimer, with the water-containing trimer falling below our noise level. The trimer including 2 water molecules is illustrated in Fig. 4b and its computed conductance falls a couple of orders of magnitude below the experimental noise floor. From this we conclude that the peaks experimentally observed in Fig. 2b correspond to water-containing monomer and dimer species. Note that these appear as two pairs of peaks. In Fig. 2b these have been labelled as one pair of peak at between $\sim 10^{-1}$–$10^{-2} G_0$ M_{H_2O}, M'_{H_2O} and a pair at significantly lower conductance (close to $10^{-4} G_0$) labelled as D_{H_2O} and D'_{H_2O}. The conductance values and their break-off distances in the 2-D histogram in Fig. 2d justify their assignment to water-containing monomer and dimer species, respectively. We ascribe the significant conductance peak splitting for both monomer and dimer species observed in the histograms in Fig. 2b to different H-bonding conformers in the junction (more details in the ESI‡). We repeated the calculations for benzimidazole, and a similar behaviour was found, albeit with slightly different conductance values (see ESI‡).

3. Conclusions

In conclusion, we demonstrated here the formation of oligomeric, hydrogen bonding chains of imidazolic compounds formed *in situ* during a break-junction experiments. This resulted in an unexpectedly complex conductance "spectrum" for such a simple, 5-member heterocyclic compound. In addition to the formation of imidazole dimers and trimers, we also observed, in aqueous environment, the formation of junctions incorporating H-bonded water. For the junctions to be stable at room temperature, the energetics of structural dissociation must be well above k_BT at room temperature. However, many compounds which have been measured as single-entity junctions in the literature might be capable of forming H-bonded chains, but evidence of *in situ* formation of oligomeric entities during a break-junction experiment is scarce. Examples of such oligomerisation processes available in the literature are limited to those involving coordination or chemical bonds, such as metallopolymers formed by abstraction of metal atoms from the two electrodes,[37] spontaneous dimerization of organotin compounds,[38] and, recently, field-induced catalytic oligomerisation of terminal anilines.[39] We believe the peculiar behaviour of imidazole can be attributed to its particularly high moment of dipole, measured at 3.67 D (as comparison, H_2O = 1.83; HCN = 2.98; acetonitrile = 3.44). The dipole is oriented in the NH → N direction, and therefore optimally arranged with the electric field induced by the tip–substrate bias to assist the formation, stabilisation and ordering of the imidazolic chains, thereby allowing them to be assemble in the junction at room temperature.

4. Methods

4.1 Chemicals

1*H*-Imidazole, benzimidazole and 1-methylimidazole (all >99% purity) were purchased from TCI UK, recrystallised from anhydrous ethanol[40] and dried in a desiccator under a vacuum of 10^{-3} bar for a week before use. Mesitylene (98%) and tetrahydrofuran were purchased from MilliporeSigma, dried with 4 Å molecular sieves[41] and degassed by purging with Ar gas for 1 hour before use. Milli-Q water was obtained from a Merck Millipore Elix water purification system and tested for resistivity ρ > 18 MΩ cm before use. Deuterium oxide was purchased from MilliporeSigma (99% atom D) and used without further purification.

4.2 Scanning tunnelling microscopy break junction measurements

We used a modified Keysight Technologies 5500 SPM, equipped with a home-built 4-channel transimpedance amplifier based on the design of Mészáros *et al.*[42] Data was acquired with a National Instruments NI9215 USB cDAQ, at 10 kSa s^{-1}. STM tips were cut from a spool of 99.99+% Au wire, purchased from Goodfellow Cambridge Ltd. Substrates used in this study were 200 nm Au films evaporated on freshly cleaved mica. We fabricated the junctions by repeatedly crashing the STM tip into the substrate and then withdrawing it at a constant speed of 20 nm s^{-1}, in a solution of the molecule of interest (1 mM concentration), at constant sample bias (200 mV). The signals (in V) from the transimpedance amplifier are the converted into current (I), and conductance is calculated using Ohm's law ($G = I/V$), as a function of the quantum of conductance $G_0 = 2e^2/h \cong 77.48$ μS. Each indentation-withdrawal cycle results therefore in a conductance *vs.* electrode separation trace, which is aligned to the rupture of the metallic nanocontact at $0.5G_0$ and thousands of these traces are compiled into histograms and density plots without further data selection or processing. Additional details on the instrument used in this study and the data acquisition/analysis process can be found in our previous publications.[43,44]

4.3 Computational methods

The relaxed geometry of the isolated molecule is obtained using the DFT code SIESTA,[45,46] so that the force on all atoms is less than 0.01 eV $Å^{-1}$. We used double-ζ basis set with polarization and norm-conserving pseudopotentials. Real space grid cut off is 150 Ry. We employed the GGA exchange–correlation functional with PBE parameterisation.[47] To calculate the conductance, geometry-optimized molecule is placed between two Au electrodes consisting of seven principle layers, with 12 Au atoms and an atomically sharp tip. We then further relaxed the geometry and we obtained the mean-field Hamiltonian and overlap matrix of the system. The transport code GOLLUM[48] was then used to calculate $T(E)$. The conductance is then obtained by

$$G = \frac{2e^2}{h}\int T(E)\frac{\partial f(E,T)}{\partial E}\mathrm{d}E \quad (1)$$

$$(E,T) = \left[e^{\frac{E-E_F}{k_B T}}+1\right]^{-1} \quad (2)$$

where k_B is the Boltzmann's constant and T is the temperature.

Conflicts of interest

The authors declare no competing financial interests.

Acknowledgements

We thank EPSRC for support (grants EP/M005046/1, EP/M029522/1, EP/M014452/1, EP/M014169/1, EP/P027156/1 and EP/N03337X/1). This work was additionally supported by the European Commission through the FET Open project 767187 (QuIET) and the EU project "Bac-to-Fuel". S. S. thanks the Leverhulme Trust for funding (Early Career Fellowship ECF-2018-375). H. S. thanks UKRI for funding (Future Leaders Fellowship MR/S015329/1). A. V. thanks the Royal Society for funding (URF/R1/191241). C. W. acknowledges funding from the China Scholarship Council (grant no. 201806860023).

References

1 L. A. Baker, *J. Am. Chem. Soc.*, 2018, **140**, 15549–15559.
2 M. Sotomayor and K. Schulten, *Science*, 2007, **316**, 1144–1148.
3 B. Xu and N. Tao, *Science*, 2003, **301**, 1221–1223.
4 M. A. Reed, C. Zhou, C. J. Muller, T. P. Burgin and J. M. Tour, *Science*, 1997, **278**, 252–254.
5 C. Evangeli, K. Gillemot, E. Leary, M. T. González, G. Rubio-Bollinger, C. J. Lambert and N. Agraït, *Nano Lett.*, 2013, **13**, 2141–2145.
6 P. T. Bui, T. Nishino, Y. Yamamoto and H. Shiigi, *J. Am. Chem. Soc.*, 2013, **135**, 5238–5241.
7 S. Martín, I. Grace, M. R. Bryce, C. Wang, R. Jitchati, A. S. Batsanov, S. J. Higgins, C. J. Lambert and R. J. Nichols, *J. Am. Chem. Soc.*, 2010, **132**, 9157–9164.
8 S. Wu, M. T. González, R. Huber, S. Grunder, M. Mayor, C. Schönenberger and M. Calame, *Nat. Nanotechnol.*, 2008, **3**, 569–574.
9 T. Nishino, N. Hayashi and P. T. Bui, *J. Am. Chem. Soc.*, 2013, **135**, 4592–4595.
10 C. Zhou, X. Li, Z. Gong, C. Jia, Y. Lin, C. Gu, G. He, Y. Zhong, J. Yang and X. Guo, *Nat. Commun.*, 2018, **9**, 807.
11 S. Chang, J. He, L. Lin, P. Zhang, F. Liang, M. Young, S. Huang and S. Lindsay, *Nanotechnology*, 2009, **20**, 185102.
12 B. M. Craven, R. K. McMullan, J. D. Bell and H. C. Freeman, *Acta Crystallogr., Sect. B: Struct. Crystallogr. Cryst. Chem.*, 1977, **33**, 2585–2589.
13 A. Lukton, *Nature*, 1961, **192**, 422–424.
14 G. Will, *Nature*, 1963, **198**, 575–575.
15 T. Ueda, S. Nagatomo, H. Masui, N. Nakamura and S. Hayashi, *Z. Naturforsch., A: Phys. Sci.*, 1999, **54**, 437–442.
16 A. Cammers and S. Parkin, *CrystEngComm*, 2004, **6**, 168–172.
17 A. Kawada, A. R. McGhie and M. M. Labes, *J. Chem. Phys.*, 1970, **52**, 3121–3125.
18 Y. Sunatsuki, H. Ohta, M. Kojima, Y. Ikuta, Y. Goto, N. Matsumoto, S. Iijima, H. Akashi, S. Kaizaki, F. Dahan and J.-P. Tuchagues, *Inorg. Chem.*, 2007, **43**, 4154–4171.
19 F. Lambert, C. Policar, S. Durot, M. Cesario, L. Yuwei, H. Korri-Youssoufi, B. Keita and L. Nadjo, *Inorg. Chem.*, 2007, **43**, 4178–4188.

20 L. Wang, L. Zhao, M. Liu, R. X. Chen, Y. Yang and Y. X. Gu, *Sci. China: Chem.*, 2012, **55**, 2115–2122.

21 Y. I. Kuznetsov and L. P. Kazansky, *Russ. Chem. Rev.*, 2008, **77**, 219–232.

22 B. H. Loo, Y. Tse, K. Parsons, C. Adelman, A. El-Hage and Y. G. Lee, *J. Raman Spectrosc.*, 2006, **37**, 299–304.

23 W. N. Richmond, P. W. Faguy and S. C. Weibel, *J. Electroanal. Chem.*, 1998, **448**, 237–244.

24 T. Fu, S. Smith, M. Camarasa-Gómez, X. Yu, J. Xue, C. Nuckolls, F. Evers, L. Venkataraman and S. Wei, *Chem. Sci.*, 2019, **68**, 42–61.

25 Y. Isshiki, S. Fujii and T. Nishino, *Phys. Chem. Chem. Phys.*, 2018, **20**, 7947–7952.

26 S. Kaneko, R. Takahashi, S. Fujii, T. Nishino and M. Kiguchi, *Phys. Chem. Chem. Phys.*, 2017, **19**, 9843–9848.

27 A. I. Yanson, G. R. Bollinger, H. E. van den Brom, N. Agraït and J. M. van Ruitenbeek, *Nature*, 1998, **395**, 783–785.

28 S. Y. Quek, M. Kamenetska, M. L. Steigerwald, H. J. Choi, S. G. Louie, M. S. Hybertsen, J. B. Neaton and L. Venkataraman, *Nat. Nanotechnol.*, 2009, **4**, 230–234.

29 J. Y. Shin, Y. L. Wang, S. A. Yamada, S. T. Hung and M. D. Fayer, *J. Phys. Chem. B*, 2019, **123**, 2094–2105.

30 D. A. Carter, J. E. Pemberton and K. J. Woelfel, *J. Phys. Chem. B*, 2002, **102**, 9870–9880.

31 P. Dash and R. W. J. Scott, *Chem. Commun.*, 2009, 812.

32 D. Murai, T. Nakazumi, S. Fujii, Y. Komoto, K. Tsukagoshi, C. Motta and M. Kiguchi, *Phys. Chem. Chem. Phys.*, 2014, **16**, 15662–15666.

33 A. R. R. P. Almeida and M. J. S. Monte, *J. Chem. Thermodyn.*, 2014, **77**, 46–53.

34 R. Landauer, *IBM J. Res. Dev.*, 1957, **1**, 223–231.

35 V. Fatemi, M. Kamenetska, J. B. Neaton and L. Venkataraman, *Nano Lett.*, 2011, **11**, 1988–1992.

36 D. C. Milan, O. A. Al-Owaedi, M.-C. Oerthel, S. Marqués-González, R. J. Brooke, M. R. Bryce, P. Cea, J. Ferrer, S. J. Higgins, C. J. Lambert, P. J. Low, D. Z. Manrique, S. Martin, R. J. Nichols, W. Schwarzacher and V. M. García-Suárez, *J. Phys. Chem. C*, 2016, **120**, 15666–15674.

37 A. Vladyka, M. L. Perrin, J. Overbeck, R. R. Ferradás, V. García-Suárez, M. Gantenbein, J. Brunner, M. Mayor, J. Ferrer and M. Calame, *Nat. Commun.*, 2019, **10**, 262.

38 Z.-L. Cheng, R. Skouta, H. Vazquez, J. R. Widawsky, S. Schneebeli, W. Chen, M. S. Hybertsen, R. Breslow and L. Venkataraman, *Nat. Nanotechnol.*, 2011, **6**, 353–357.

39 Y. Zang, I. Stone, M. S. Inkpen, F. Ng, T. H. Lambert, C. Nuckolls, M. L. Steigerwald, X. Roy and L. Venkataraman, *Angew. Chem., Int. Ed.*, 2019, 1–6.

40 W. L. F. Armarego and C. L. Chai, *Purification of Laboratory Chemicals*, Butterworth-Heinemann, Oxford, 6th edn, 2003.

41 D. B. G. Williams and M. Lawton, *J. Org. Chem.*, 2010, **75**, 8351–8354.

42 G. Mészáros, C. Li, I. Pobelov and T. Wandlowski, *Nanotechnology*, 2007, **18**, 424004.

43 R. J. Brooke, C. Jin, D. S. Szumski, R. J. Nichols, B. Mao, K. S. Thygesen and W. Schwarzacher, *Nano Lett.*, 2015, **15**, 275–280.

44 D. C. Milan, M. Krempe, A. K. Ismael, L. D. Movsisyan, M. Franz, I. Grace, R. J. Brooke, W. Schwarzacher, S. J. Higgins, H. L. Anderson, C. J. Lambert, R. R. Tykwinski and R. J. Nichols, *Nanoscale*, 2017, **9**, 355–361.

45 E. Artacho, E. Anglada, O. Diéguez, J. D. Gale, A. García, J. Junquera, R. M. Martin, P. Ordejón, J. M. Pruneda, D. Sánchez-Portal and J. M. Soler, *J. Phys.: Condens. Matter*, 2008, **20**, 064208.

46 J. M. Soler, E. Artacho, J. D. Gale, A. García, J. Junquera, P. Ordejón and D. Sánchez-Portal, *J. Phys.: Condens. Matter*, 2002, **14**, 2745–2779.

47 R. Peverati, Y. Zhao and D. G. Truhlar, *J. Phys. Chem. Lett.*, 2011, **2**, 1991–1997.

48 J. Ferrer, C. J. Lambert, V. M. García-Suárez, D. Z. Manrique, D. Visontai, L. Oroszlany, R. Rodríguez-Ferradás, I. Grace, S. W. D. Bailey, K. Gillemot, H. Sadeghi and L. A. Algharagholy, *New J. Phys.*, 2014, **16**, 093029.